PRAMANA
— journal of
physics

Vol. 58, No. 1
January 2002
pp. 91–100

Strong anisotropy in the low temperature Compton profiles of electron momentum distribution in α-Ga metal

B P PANDA and N C MOHAPATRA*
Department of Physics, Chikiti Mahavidyalaya, Chikiti 761 010, India
*Department of Physics, Berhampur University, Berhampur 760 007, India

MS received 12 April 2001; revised 1 September 2001

Abstract. Compton profiles of momentum distribution of conduction electrons in the orthorhombic phase of α-Ga metal at low temperature are calculated in the band model for the three crystallographic directions (100), (010), and (001). Unlike the results at room temperature, previously reported by Lengeler, Lasser and Mair, the present results show strong anisotropy in the Compton profiles with the momentum distribution along (001) direction being substantially different from the other two directions. While experimental data on Compton profiles at low temperatures are not available for comparison with theory, the resistivity data in α-Ga at low temperature strongly support this anisotropic behaviour. Besides, the electronic heat capacity constant γ available from both experiment and present calculation suggests that the conduction electron distribution at low temperature in the orthorhombic phase is markedly different from the free-electron-like-distribution at room temperature, thus lending additional support to anisotropic behaviour of Compton profiles. It would be nice to have Compton profiles data from experiment at low temperature for direct comparison with theory. It is hoped that the present work would stimulate enough interest in that direction.

Keywords. Strong anisotropy; Compton profiles; α-gallium; low temperature.

PACS Nos 72.60;78.70;71.25.

1. Introduction

It is well known that the Compton profile of free-electron momentum distribution is isotropic with the profile described by an inverse parabolic function. The momentum distribution in solids, on the other hand, shows departure from the isotropic behaviour, the degree of departure being intimately connected with the electronic structure. Therefore, a study of Compton profiles of electron momentum distribution in solids provides useful information as to the electronic structure of solids. For this reason it has been a subject of extensive study both in theory and experiments.

On the experimental side, measurements of profiles of momentum distribution are carried out using both X-rays [1,2] and γ-rays [3,4]. While in some measurements [1–3] the dependence of profiles on crystallographic direction is not available, in others [4], the Compton profiles are determined along different crystallographic directions. It is the latter

experiment which provides a better insight as to the extent of departure of the Compton profiles from the isotropic free-electron result.

On the theoretical side, Compton profiles in solids are available from calculations using renormalized free-atom (RFA) model [3], band model [5–7] and quantum Monte Carlo procedure [8,9]. Out of these the RFA model is the least realistic one.

In α-Ga metal, results of Compton profiles are available from experiment [4] only at room temperature. These show near isotropy and have been explained by the RFA model [4]. The results lead to the conclusion that the conduction electron distribution at room temperature in α-Ga is free-electron like.

However, at low temperature such as 77 K, the resistivity data measured [10,11] in α-Ga suggest strong anisotropic behaviour with the resistivity along the (001) crystallographic direction being substantially larger than those along (100) and (010) directions. This makes one to believe that the conduction electron distribution at low temperature shows strong departure from the free-electron-like behaviour observed at room temperature. The measurements [12–15] of electronic specific heat constant γ at low temperature lend additional support to this conclusion.

The reasons for taking up α-Ga for the calculation of Compton profiles in the orthorhombic phase at low temperature are two-fold. The first is to fulfill the need to have these results which are heretofore not available in the literature and the second is to see if the Compton profiles, like the resistivity data, show strong anisotropic behaviour at low temperature.

In the present work the Compton profiles are determined in the band model which is more realistic than the RFA model [3]. Momentum distributions are calculated along the three crystallographic directions, (100), (010) and (001). The results indeed show significant anisotropy with the profile along (001) direction being substantially different from the other two directions.

The paper is organized as follows: In §2, the theory of Compton profiles is briefly described. Section 3 deals with the results of the present calculation. In §4, conclusions are summarized.

2. Theory

The calculation of electron momentum distribution in band model invariably uses the impulse approximation [16], according to which the profile function along any arbitrary direction $\hat{k}$ is expressed [5–7] as

$$J_{\hat{\kappa}}(q) = \frac{\Omega}{(2\pi)^3}\int \mathrm{d}^3 p \rho(\vec{p})\,\delta(q - \vec{p}\cdot\hat{\kappa}), \tag{1}$$

where Ω is the volume of the unit cell, $\vec{p}$ the momentum of electron and ρ the momentum probability distribution function. The latter is related to the Fourier transform of electron wave function in co-ordinate representation.

In procedures of energy band calculations using model potential, as is the case in the present work, the conduction electron wave function is expressed [6] as

$$\Psi_t(\vec{g},\,\vec{r}) = \sum_{\vec{K}} C_t(\vec{g},\vec{K})\left[\mathrm{PW}(\vec{g}+\vec{K},\,\vec{r}) - \sum_i \langle\phi_i(\vec{g})|\mathrm{PW}(\vec{g}+\vec{K})|\rangle\,\phi_i(\vec{g},\vec{r})\right], \tag{2}$$

where t denotes the band index, $\vec{g}$ is a wave vector in the Brillouin zone (BZ), $\vec{K}$ is a reciprocal lattice vector, PW and ϕ_i are the normalized plane wave and the tight- binding functions respectively and C_t are the coefficients of combination. Both the C_t coefficients and the energy $E_t(\vec{g})$ of the state Ψ_t are obtained as solutions of a standard secular equation.

The squared magnitude of the Fourier transform of Ψ_t, summed over all the occupied states of band electrons, generates $\rho(\vec{p})$. Using the latter in the integral in eq. (1), the profile function for different values of momentum q is evaluated for any given crystallographic direction $\hat{\kappa}$.

The detailed expressions for $\rho(\vec{p})$ and $J_{\hat{\kappa}}(q)$ are available in the work of Panigrahi and Mohapatra [6]. To avoid repetition, those expressions are not reproduced here. The interested reader may refer to the previous work [13] for details.

However, we have further simplified the final expression for $J_{\hat{\kappa}}(q)$ given in ref. [6] by splitting it into three parts which show the individual contribution arising from the plane wave, hybrid (i.e PW–TB and TB–PW) and the tight-binding parts of $\rho(\vec{p})$.

It may be noted that the net $J_{\hat{\kappa}}(q)$ is expressed [6] as

$$J_{\hat{\kappa}}(q) = \frac{\mathrm{d}F_{\hat{\kappa}}(q)}{\mathrm{d}q}, \tag{3}$$

where the expression for the function $F_{\hat{\kappa}}(q)$ is worked out in [6]. Separating $F_{\hat{\kappa}}(q)$ into contributions from the plane wave, hybrid and the tight-binding parts, the contributions per atom arising from these parts have been worked out and are given below:

$$F_{\hat{\kappa}}^{\mathrm{PW}}(q) = \frac{2}{\zeta}\sum_{\vec{g}}\omega_{\vec{g}}\left[\sum_{\vec{K}}\left\{\sum_{\alpha}\theta\left(q-(\vec{g}+\vec{K})\cdot\alpha\hat{\kappa}\right)\right\}\left\{\sum_{t}|C_t(\vec{g},\vec{K})|^2\right\}\right], \tag{4}$$

$$\begin{aligned} F_{\hat{\kappa}}^{\mathrm{hy}}(q) = -\frac{32\pi\zeta}{\Omega}\sum_{\vec{g}}\omega_{\vec{g}}\sum_{\vec{K}}\sum_{\vec{K}'}\Bigg[&\left\{\sum_{t}C_t(\vec{g},\vec{K})C_t(\vec{g},\vec{K}')\right\} \\ &\times\left\{\sum_{nl}(2l+1)I_{nl}(|\vec{g}+\vec{K}|)I_{nl}(|\vec{g}+\vec{K}'|)P_l\left(\cos(\beta_{K,\vec{K}'})\right)\right\} \\ &\times\left\{\sum_{\alpha}\theta(q-(\vec{g}+\vec{K})\cdot\alpha\hat{\kappa})S(\alpha\vec{K})S(\alpha\vec{K}')\right\}\Bigg], \end{aligned} \tag{5}$$

and

$$\begin{aligned} F_{\hat{\kappa}}^{\mathrm{TB}}(q) = -\left(\frac{32\pi^2}{\zeta\Omega_0^2}\right)\sum_{\vec{g}}\omega_{\vec{g}}\sum_{s}S^2(\vec{K}_s)\sum_{\alpha}\theta\left\{q-(\vec{g}+\vec{K}_s)\cdot\alpha\hat{\kappa}\right\} \\ \times\sum_{t}\Bigg[\sum_{\vec{K}}C_t(\vec{g},\vec{K})S(\alpha\vec{K})\sum_{nl}(2l+1)P_l\left\{\cos(\beta_{\vec{K}_s\vec{K}})\right\} \\ \times I_{nl}(|\vec{g}+\vec{K}_s|)I_{nl}(|\vec{g}+\vec{K}|)\Bigg]^2, \end{aligned} \tag{6}$$

where Ω_0 is the volume per atom, ζ is the number of atoms per unit cell, $\omega_{\vec{g}}$ is the weighing factor associated with the $\vec{g}$ in the BZ, $\beta_{\vec{K}\vec{K}'}$ is the angle between the vector $(\vec{g}+\vec{K})$ and

$(\vec{g}+\vec{K}')$, S is the structure factor, α is the operator representing the point symmetry of the lattice, P_l is the Legendre polynomial of order l and $I_{nl}(k)$ is the radial integral of the product of the radial part of the atomic core function and the spherical Bessel function $j_l(kr)$. The latter integral is defined in eq. (8) of [6]. The θ-function appearing in eqs (4)–(6) is the standard step function. The $\vec{g}$ sum in each of the eqs (4)–(6) is taken over the irreducible part of the BZ.

The purpose of splitting $F_{\hat{\kappa}}(q)$ into three parts as given in eqs (4)–(6) is to study the relative importance of the individual contributions. We would like to remark here that if the $\vec{K}$ vectors used in the calculation are the members of the star of $\vec{K}$, the expressions in eqs (4)–(6) get simplified further by the symmetry consideration. The simplification involves replacing all the $S(\alpha\vec{K})$ by $S(\vec{K})$ as eq. (10) of [6] suggests. But in the calculations using $\vec{K}$ vectors from an incomplete star of $\vec{K}$, one has to use $S(\alpha\vec{K})$ instead of $S(\vec{K})$. However, if one or two $\vec{K}$ vectors from the star are missed, the error that results from the replacement of $S(\alpha\vec{K})$ by $S(\vec{K})$ is usually negligible. We wish to write down the equations for $J(q)$ and $F(q)$ in the free-electrons case for comparison with those in the metal. The profile function per atom in the free electron case is given by

$$J(q) = \begin{cases} \frac{\Omega_0}{(2\pi)^2}\left(k_{\mathrm{F}}^2 - q^2\right), & |q| < k_{\mathrm{F}} \\ 0, & \text{otherwise,} \end{cases} \tag{7}$$

where k_{F} is the free-electron Fermi wave vector. The $F(q)$ function which is related to $J(q)$ by eq. (3) is given for the free electron by

$$F(q) = \begin{cases} \frac{\Omega_0}{(2\pi)^2}\left(k_{\mathrm{F}}^2 - \frac{q^2}{3}\right)q + 1.5, & |q| \le k_{\mathrm{F}} \\ 0, & q < -k_{\mathrm{F}} \\ 3, & q > k_{\mathrm{F}}\,. \end{cases} \tag{8}$$

3. Results and discussion

α-Ga has orthorhombic structure [17] and is characterized by the D_{2h} group of point symmetry. The primitive cell has four atoms. The lattice parameters corresponding to low temperature (i.e. 2.35 K) orthorhombic phase are [17]: $a = 8.53230$ atomic units (au), $b = 8.48128$ au, $c = 14.42202$ au, $u = 0.0785$, and $v = 0.1525$. Energy band calculations are carried out using the non-local model potential of Appapillai and Williams [18]. Energies and wave functions are computed at 108 $\vec{g}$ points suitably chosen in one-eighth irreducible part of the BZ. For this purpose, the wedge shaped irreducible part of the BZ is divided into six equidistant parallel planes by slicing along the c-axis. Each plane is divided into eighteen parts consisting of nine rectangles and nine triangles. The rectangles are of equal area, so are the triangles. But the area of a rectangle is different from the area of a triangle. The centroids of parallelopiped and the triangular prisms formed between successive planes are chosen as the representative $\vec{g}$ points, 108 in total in the one-eighth irreducible part of the BZ, at which energies and eigenfunctions are calculated. This amounts to having energy and eigenfunctions at 864 $\vec{g}$ points in the full BZ. To each

one of the representative $\vec{g}$ points, a weighing factor $w_{\vec{g}}$ in proportion to the volume that it represents, is assigned. The sum of $w_{\vec{g}}$ over 864 $\vec{g}$ points is equal to 1, as it should.

At each one of the representative $\vec{g}$ points, the model wave function is expanded in 23 plane waves corresponding to the shortest 23 wave vectors $|\vec{g}+\vec{K}|$ for that $\vec{g}$ vector. With this choice the convergence of energy and eigenfunctions is found to be good. The energies of the occupied bands have converged to within 0.001 Ryd. The conduction electron wave function $\psi_t(\vec{g},\vec{r})$ is constructed [6] from the model wave function by orthogonalizing the latter to the core electron states, each one of which is represented by a single tight-binding function formed from the corresponding atomic core state. The atomic core states used for this purpose are the Hartree–Fock wave functions of Clementi [19].

Using the energies at 108 $\vec{g}$ points, the Fermi energy E_{F}, the density of states at E_{F} and the electronic specific heat constant γ have been determined and compared with those available from other calculations [12] and experiments [12–15]. These results are summarized in table 1. In this table, the results listed in column 4 are from the APW calculation reported by Wood [12]. While the Fermi energy E_{F} has nearly the same value, the density of states and the γ parameter are widely different. It is gratifying to note that the γ parameter in the present work falls within the experimental [12–15] range while those from free-electron model and the APW calculation [12] are markedly different. That the model potential method, as used in the present work, is expected to give better results than the APW method in α-Ga is supported by the statements made by Reed [10]. The reasons offered by Reed [10] for this case are that the muffin-tin potential [10,12] used in α-Ga approximates 60% of the total cell volume with a constant potential, leaving only 40% of the volume inside the APW spheres. That the present results of density of states and γ are substantially different from the free-electron values indicates strong anisotropy in the momentum distribution of conduction electrons in α-Ga at low temperature.

Having determined the Fermi energy and the coefficients $C_t(\vec{g},\vec{K})$ for all the occupied bands at 108 representative $\vec{g}$ points in the irreducible part of the BZ, the contributions to $F_{\hat{\kappa}}(q)$ are evaluated using eqs (4)–(6). The ζ parameter is equal to 4 as the primitive cell in α-Ga contains four atoms. The sum over α, which consists of eight symmetry operations, along with the sum over $\vec{g}$ in the $\frac{1}{8}$th irreducible part of the BZ account for the contribution from the full BZ.

The $F_{\hat{\kappa}}$ function by its nature is a monotonically increasing function of q, which saturates at large q. But while evaluating these functions from eqs (4)–(6), each one of which involves the step function θ, caution is to be exercised in choosing the mesh size in q. For

Table 1. E_{F}, the Fermi energy, $G(E_{\mathrm{F}})$, the density of states at E_{F}, γ, the electronic specific heat constant in α-Ga metal from different calculations and experiment. E_{F} is expressed in Rydberg, G(E_{F}) in number of states/cell/Rydberg and γ in mJ/mole/°K^2.

	Theory				Expt.
Parameters	Present result	[10]	[12]	Free-electron result	[12–15]
E_{F}	0.7702	0.7770	0.8000	0.7739	–[a]
G(E_{F})	14.5865	–	21.4838	23.2570	–
γ	0.6327	–	0.9000	1.0088	0.60–0.75

[a]The '–' in the above columns denotes non-availability of the corresponding results.

Table 2. Present results of Compton profiles of electron momentum distribution of conduction electrons in α-Ga at low temperature. $J_{100}(q)$, $J_{010}(q)$, $J_{001}(q)$ denote the profiles along (100), (010) and (001) directions respectively. $J_{\text{free}}(q)$ gives the free-electron values. All the quantities are expressed in atomic units.

q	$J_{100}(q)$	$J_{010}(q)$	$J_{001}(q)$	$J_{\text{free}}(q)$
0.0	2.529	2.516	3.747	2.558
0.1	2.463	2.506	2.047	2.524
0.2	2.331	2.192	1.640	2.425
0.3	2.151	1.909	2.969	2.260
0.4	1.897	1.936	2.107	2.029
0.5	1.611	1.801	1.189	1.731
0.6	1.271	1.373	1.372	1.368
0.7	0.838	0.807	1.100	0.938
0.8	0.407	0.299	0.348	0.443
0.9	0.138	0.067	0.112	0.000
1.0	0.060	0.046	0.128	0.000
1.1	0.045	0.042	0.036	0.000
1.2	0.033	0.036	0.032	0.000

example, the quantity $(\vec{g}+\vec{K})\cdot\alpha\hat{\kappa}$ in the step function of eq. (4) does not vary continuously due to finiteness of the chosen set of $\vec{g}$ vectors and $\vec{K}$ vectors. Thus, for all values of q which fall between two successive values of $(\vec{g}+\vec{K})\cdot\alpha\hat{\kappa}$, $F_{\hat{\kappa}}(q)$ remains unchanged contrary to its monotonically increasing nature.

To avoid errors from this effect we first determined the number of distinct lengths $(\vec{g}+\vec{K})\cdot\alpha\hat{\kappa}$ arising from all possible values of $\vec{g}, \vec{K}$ and $\alpha\hat{\kappa}$, which turn out to be 48, 48 and 60 for (100), (010), and (001) directions respectively. The $F_{\hat{\kappa}}$ functions are determined at these lengths used as q values. As the latter q values form a non-uniform mesh, the $F_{\hat{\kappa}}$ functions at these q values are used to obtain the $F_{\hat{\kappa}}$ function for q values chosen in a uniform mesh by the trapezoidal rule of interpolation. To obtain the profile function $J_{\hat{\kappa}}(q)$ which is related to $F_{\hat{\kappa}}(q)$ by eq. (3), a four-point numerical differentiation formula [20] is used to calculate the first derivative of the corresponding $F_{\hat{\kappa}}(q)$, generated at q values in a uniform mesh.

The results of the profile function $J_{\hat{\kappa}}(q)$ are presented in table 2 for the three crystallographic directions (100), (010) and (001) in columns 2, 3 and 4 respectively. The free-electron $J(q)$, which is isotropic, is also listed in column 5 of this table for comparison.

In addition, the $F_{\hat{\kappa}}$ functions for the three crystallographic directions are plotted in figure 1, while the profile functions $J_{\hat{\kappa}}(q)$ for the said directions are plotted in figure 2. In each figure, the free-electron result is also plotted. However, in figure 1 to keep the three solid lines well separated from each other, the functions actually plotted are $0.85\times F_{100}$, $0.75\times F_{010}$ and $1.25\times F_{001}$ instead.

It is clear from both table 2 and figure 2 that the profile function along the (001) direction is substantially different from not only the free-electron result but also those along (100) and (010) directions. Similar anisotropy was observed in the d.c. resistivity [10] in α-Ga at low temperature. The latter is attributed [10,21] to large scale deformation of the free-electron Fermi surface, especially along g_z, that is the (001) direction and to an accompanying energy gap at the Fermi level. This gap, according to Heine [21], is in some

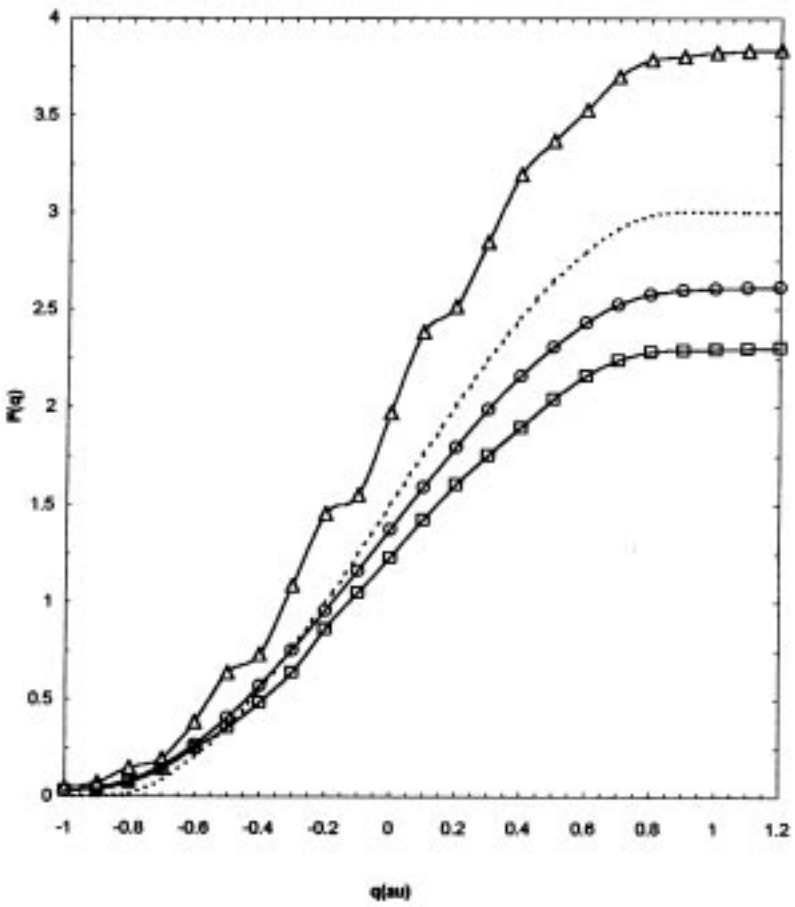

Figure 1. Variation of $F_{\hat{\kappa}}(q)$ in α-Ga metal at low temperature. Dashed line denotes the isotropic free-electron result. Solid lines labelled by symbols ◯, □, and △ represent band model results along (100), (010), (001) directions respectively. For keeping the three solid lines well separated from each other, the functions $0.85 \times F_{100}$, $0.75 \times F_{010}$ and $1.25 \times F_{001}$ are plotted instead of the respective F.

sense a measure of covalency. A detailed Fermi surface calculation in α-Ga by Reed [10] supports Heine's [21] prediction. It is the covalency which accounts for the larger d.c. resistivity along (001) direction. We suspect that the relatively large deformation of the free-electron Fermi surface along the (001) direction leads to the Compton profile along this direction substantially different from the free-electron result.

The Compton profile data from experiment at room temperature [4], on the other hand, suggest that the conduction electron distribution at this temperature is free-electron like. This has been explained reasonably well by a spherically averaged $J(q)$ calculated by Lengeler *et al* [4] in the RFA model [3] where the latter authors replaced the actual orthorhombic structure of α-Ga by a pseudo-tetragonal structure. The latter authors [4]

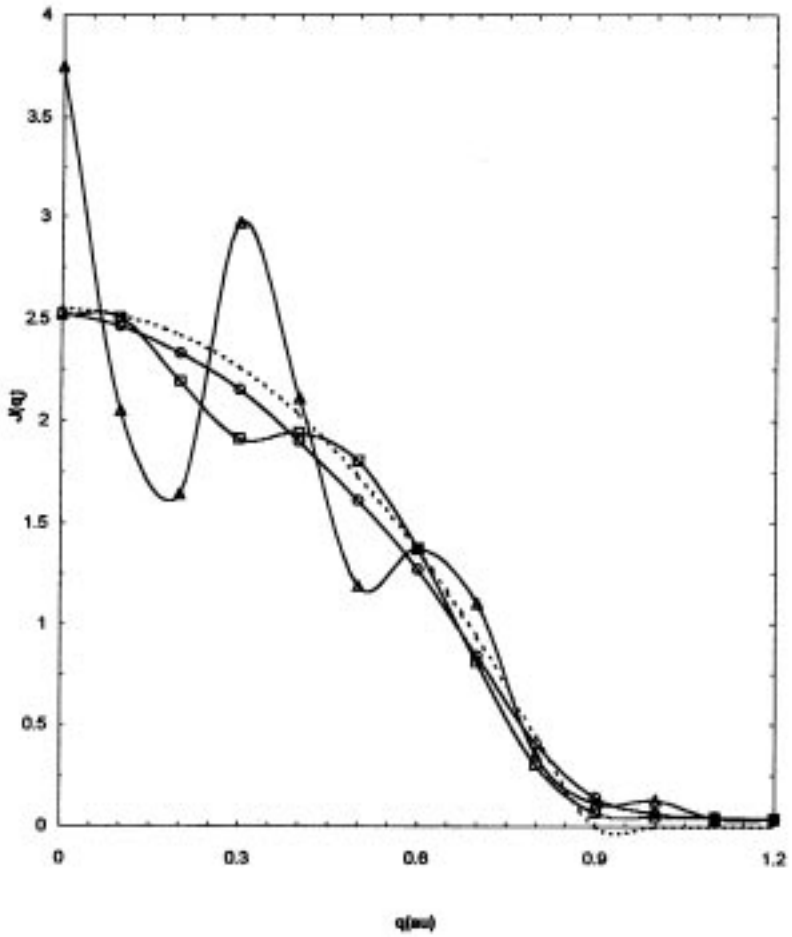

Figure 2. Variation of Compton profile $J(q)$ in α-Ga metal at low temperature. Dashed line denotes the isotropic free-electron result. Solid lines labelled by symbols ◯, □ and △ represent band model results along (100), (010) and (001) directions respectively. The free-electron result goes to zero at Fermi momentum $P_{\mathrm{F}} \approx 0.88$ au.

admit the good agreement of their calculated result with experiment as fortuitous. A better explanation for the profiles at room temperature may result from the calculation of $J_{\hat{\kappa}}(q)$ at room temperature in the band model. The latter calculation will be taken up in future as a separate work.

However, the near isotropic behaviour of experimental [4] data at room temperature, in contrast to strong anisotropy at low temperature, may be explained by the weakening of the crystal potential at high temperature. It is shown by Kasowski [22] that the form factor at any temperature T is reduced from the value at absolute zero by $\mathrm{e}^{-W_0(T)}$, the latter being the square root of the Debye–Waller factor [23]. A weaker potential tends

Table 3. Present results of the $F_{001}(q)$ from the PW, hybrid and the tight-binding parts of $\rho(\vec{p})$. All the data are expressed in atomic units.

q	$F_{001}^{\mathrm{PW}}(q)$	$F_{001}^{\mathrm{hy}}(q)$	$F_{001}^{\mathrm{TB}}(q)$	$F_{001}^{\mathrm{Tot}}(q)$
0.0	1.559	−0.056	0.072	1.575
0.1	1.901	−0.071	0.079	1.908
0.2	2.007	−0.077	0.082	2.012
0.3	2.278	−0.088	0.087	2.277
0.4	2.561	−0.099	0.094	2.555
0.5	2.699	−0.102	0.097	2.694
0.6	2.824	−0.104	0.100	2.819
0.7	2.961	−0.107	0.105	2.959
0.8	3.026	−0.107	0.109	3.027
0.9	3.038	−0.107	0.110	3.041
1.0	3.051	−0.108	0.115	3.057
1.1	3.054	−0.108	0.119	3.065
1.2	3.055	−0.108	0.120	3.067

to make the conduction electron distribution free-electron like and hence may explain the near isotropic momentum distribution.

In order to study the relative importance of the contribution to $F_{\hat{\kappa}}(q)$ from the plane wave, hybrid and the tight-binding part of $\rho(\vec{p})$, we have listed in table 3 the individual contributions along (001) direction for q lying in the range 0–1.2 au. The last column in this table lists the total contribution to $F(q)$. It is evident from this table that the plane wave contribution is the dominant one and the hybrid and the tight-binding contributions are of the same order of magnitude but of opposite sign.

In the absence of experimental results at low temperature for the orthorhombic phase, there is no direct way of judging the accuracy of the present results. However, as stated in the Introduction, indirect support to the present results comes from the anisotropic d.c. resistivity data and the specific heat constant γ. Another test for the accuracy of the present result is offered [6] by the integral

$$\int_{-\infty}^{\infty} J_{\hat{\kappa}}(q)\mathrm{d}q = N, \tag{9}$$

where N is the number of conduction electrons per atom. The integral in eq. (9), in view of eq. (3), reduces to

$$F_{\hat{\kappa}}(-\infty) - F_{\hat{\kappa}}(\infty) = N. \tag{10}$$

Considering $F_{\hat{\kappa}}(-\infty) = 0$ and that the saturation value of $F_{\hat{\kappa}}$ starts at around $q = 1.5$ au, we find $N = 3.060$, 3.060, and 3.057 for the directions (100), (010) and (001) respectively. These values are close to 3, the actual number of valance electrons per atom. It may be noted that the free-electron F function, as given in eq. (8), when used in eq. (10) gives $N = 3$ exactly, as it should.

We also remark here that unlike free-electron $J(q)$ which goes to zero at $q = P_{\mathrm{F}}$, the free-electron Fermi momentum, the $J_{\hat{\kappa}}(\vec{q})$ in metal extends beyond P_{F} with a finite but small value. This is a consequence of the band structure and electron–electron correlation effect, the latter enters the calculation through the model potential.

4. Conclusions

The Compton profiles of momentum distribution of conduction electrons in orthorhombic phase of α-Ga metal at low temperature are calculated in the band model. The results, unlike those at room temperature, show strong anisotropy with the profile along (001) crystallographic direction being markedly different from (100), (010) directions and the free-electron result. The anisotropy is believed to be due to strong deformation of the free-electron Fermi surface along the (001) direction as noticed by Heine and Reed at low temperature. Although results of Compton profiles from experiment are not available at low temperature for direct comparison with theory, the d.c. resistivity data at low temperature and the electronic specific heat constant γ indirectly lend support to the anisotropic behaviour of the Compton profiles.

It is hoped that the present work would stimulate interest for measurement of Compton profile data at low temperatures in the orthorhombic phase of α-Ga for direct comparison with the present results.

Acknowledgements

One of the authors (BPP) is grateful to the University Grants Commission, India, for financial support sanctioned for undertaking Minor Research Project.

References

[1] S Manninen, *J. Phys.* **F1**, 160 (1971)
[2] R J Weiss, *Philos. Mag.* **26**, 761 (1972)
[3] T Paakkari, K-F Berggren, R Ribberfors and V Halonen, *Phys. Rev.* **B14**, 2301 (1976)
[4] B Lengeler, R Lasser and G Mair, *Phys. Rev.* **B22**, 5718 (1980)
[5] J Rath, C S Wang, R A Tawil and J Callaway, *Phys. Rev.* **B8**, 5139 (1973)
[6] B B Panigrahi and N C Mohapatra, *J. Phys: Condens. Matter* **5**, 8557 (1993)
[7] B K Acharya and N C Mohapatra, *Pramana – J. Phys.* **43**, 391 (1994)
[8] B Kralik, P Delaney and S G Louie, *Phys. Rev. Lett.* **80**, 4253 (1998)
[9] Claudia Filippi and David M Ceperley, arxiv:Cond-mat/9808114, 11 Aug. 1998. This pre-print is retrieved from Los Alamos National Library, USA
[10] W A Reed, *Phys. Rev.* **188**, 1184 (1969)
[11] W A Reed and J A Marcus, *Phys. Rev.* **130**, 957 (1963)
[12] J H Wood, *Phys. Rev.* **146**, 432 (1966)
[13] N M Wolcott, *Bull. Am. Phys. Soc.* **1**, 289 (1956)
[14] G Seidel and D H Keesom, *Phys. Rev.* **112**, 1083 (1958)
[15] N E Phillips, *Phys. Rev.* **A134**, 385 (1964)
[16] P M Platzman and N Tzoar, *Phys. Rev.* **A139**, 410 (1965)
[17] J C Slater, G F Koster and J H Wood, *Phys. Rev.* **126**, 1307 (1962)
[18] M Appapillai and A R Williams, *J. Phys.* **3**, 759 (1973)
[19] E Clementi, *Tables of atomic functions* (White Plain, IBM, NY, 1967)
[20] K L Neilsen, *Methods in numerical analysis* (MacMillan, New York, 1967) p. 366
[21] V Heine, *J. Phys.* **C1**, 222 (1968)
[22] R V Kasowski, *Phys. Rev.* **187**, 981 (1969)
[23] R A T Lima and C T Sallis, *Phys. Rev.* **B21**, 458 (1980)